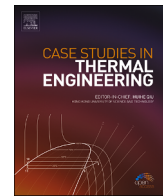




Contents lists available at ScienceDirect

# Case Studies in Thermal Engineering

journal homepage: [www.elsevier.com/locate/csite](http://www.elsevier.com/locate/csite)

## A numerical modeling of battery thermal management system using nano-enhanced phase change material in hot climate conditions

Jing Zhu<sup>a</sup>, Rishabh Chaturvedi<sup>b</sup>, Yasser Fouad<sup>c,\*</sup>, Ibrahim Albaijan<sup>d</sup>, Nizomiddin Juraev<sup>e,f</sup>, Laith H. Alzubaidi<sup>g,h,i</sup>, Ibrahim Mahariq<sup>j,k,\*\*</sup>, Abdulkareem Afandi<sup>l</sup>, Hakim A.L. Garalleh<sup>l</sup>

<sup>a</sup> School of Economics and Management, Hubei University of Automotive Technology, Shiyan, 442000, Hubei, China

<sup>b</sup> Department of Mechanical Engineering, GLA University, Mathura, India

<sup>c</sup> Department of Applied Mechanical Engineering, College of Applied Engineering, Muzahimiyah Branch, King Saud University, P.O. Box 800, Riyadh, 11421, Saudi Arabia

<sup>d</sup> Mechanical Engineering Department, College of Engineering at Al-Kharj, Prince Sattam Bin Abdulaziz University, Al Kharj, 16273, Saudi Arabia

<sup>e</sup> Researcher, Faculty of Chemical Engineering, New Uzbekistan University, Tashkent, Uzbekistan

<sup>f</sup> Scientific and Innovation Department, Tashkent State Pedagogical University, Tashkent, Uzbekistan

<sup>g</sup> College of Technical Engineering, The Islamic University, Najaf, Iraq

<sup>h</sup> College of Technical Engineering, The Islamic University of Al Diwaniyah, Al Diwaniyah, Iraq

<sup>i</sup> College of Technical Engineering, The Islamic University of Babylon, Babylon, Iraq

<sup>j</sup> Electrical and Computer Engineering Department, Gulf University for Science and Technology, Mishref, Kuwait

<sup>k</sup> Department of Medical Research, China Medical University Hospital, China Medical University, Taichung, Taiwan

<sup>l</sup> Department of Mathematical Science, College of Engineering, University of Business and Technology, Jeddah, 21361, Saudi Arabia



### ARTICLE INFO

Handling Editor: Huihe Qiu

#### Keywords:

Battery thermal management system  
Pouch battery  
NePCM  
CFD  
Hot climate

### ABSTRACT

Battery thermal management system (BTMS) is of utmost importance to ensure their safe and efficient operation. In regions with hot climates, such as Saudi Arabia, batteries are particularly susceptible to overheating, leading to performance degradation, safety risks, and potential fires. Traditional phase change materials (PCMs) have limitations in terms of slow response times and limited thermal conductivity. To overcome these challenges, nano-enhanced PCMs (NePCMs) have been developed, incorporating nanoparticles into the PCM matrix to enhance their thermal properties. This study focused on the application of NePCM, specifically RT44 and SWCNT, for BTMS of a pouch battery in hot climates. The investigation primarily centered on exploring the effects of NePCM chamber thicknesses at the top and bottom. It was expected that increasing the NePCM thickness would effectively regulate battery temperature. However, the study revealed that the thickness of the NePCM had a limited impact on battery temperature due to the dominant influence of the ambient environment. In summary, the results of this study indicate that the optimal design configuration for the NePCM chamber, in terms of thickness, consists of a bottom thickness of 10 mm and a top thickness of 15 mm.

\* Corresponding author.

\*\* Corresponding author.

E-mail addresses: [yfouad@ksu.edu.sa](mailto:yfouad@ksu.edu.sa) (Y. Fouad), [ibmohariq@gmail.com](mailto:ibmohariq@gmail.com) (I. Mahariq).

## 1. Introduction

BTMS is a critical aspect of battery technology, ensuring the safe and efficient operation of energy storage systems. In regions characterized by hot climates, such as Saudi Arabia, batteries face significant challenges due to elevated temperatures. This is because the high ambient temperatures can exacerbate the heat generated by the battery during operation [1–3]. In this respect, the extreme heat can lead to accelerated degradation, reduced performance, safety hazards, and even catastrophic events like thermal runaway and fires. Therefore, effective BTMS strategies are essential to maintain battery performance, prolong their lifespan, and ensure the safety of energy storage systems in such environments [4–6]. Conventional BTMS techniques for batteries often involve air or liquid cooling systems. However, these systems can be inefficient and susceptible to temperature fluctuations. In contrast, PCMs offer a promising alternative, providing a more effective and stable method of regulating battery temperature [7–9]. PCMs are solid-state materials that can store and release large amounts of latent heat during phase transitions, such as melting and solidification. This unique property makes them ideal for absorbing and dissipating heat from batteries, effectively maintaining their operating temperature within desired ranges [10–12]. Compared to conventional cooling systems, PCMs offer several advantages, including [13–15]:

- **High Heat Capacity:** PCMs can store significant amounts of heat energy, providing superior heat absorption capabilities compared to conventional cooling systems.
- **Stability and Durability:** PCMs are typically stable and durable materials, with minimal degradation over time, ensuring long-term BTMS effectiveness.
- **Passive Operation:** PCMs operate passively, without the need for external energy sources, reducing energy consumption and complexity.

Study [16] proposed 9 new branch fin designs for a PCM-BTMS to enhance heat transfer in lightweight metal fins. According to their results, Optimal fins maintained average cell temperature at 318.15 K, improving heat transfer by 14.98 %, extending operating time by 131.5 %, and reducing system weight by 10.28 %. Sudhakaran et al. [17] investigated the cooling performance of BTMS in Electric Vehicles (EVs) using PCM. Capric Acid and RT-35 exhibited promising BTMS capabilities. The results showed that the most

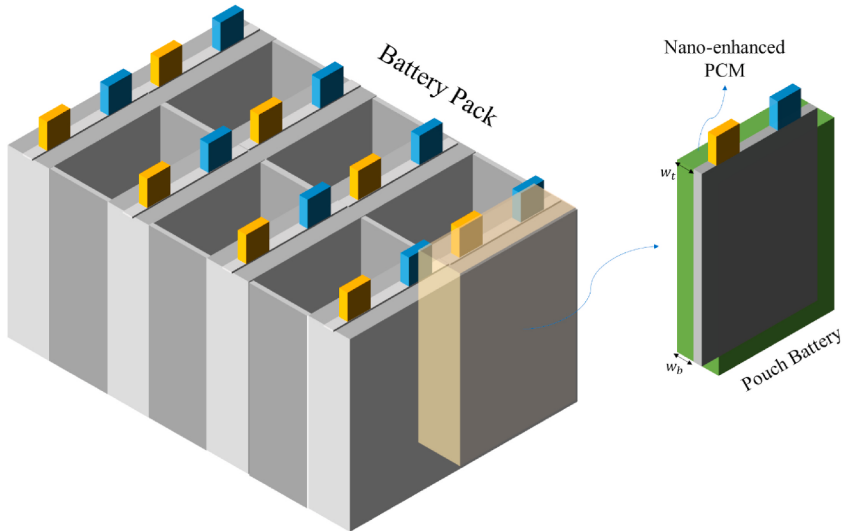


**Fig. 1.** A battery pack designed for LIPBs immersed into NePCM.

**Table 1**

The key specifications of LIPB with acceptable operating temperature for hot environments.

Specification	Value
Height	231mm
Width	161mm
Thickness	10mm
Density	2255 $\frac{kg}{m^3}$
Specific heat capacity	1067 $\frac{J}{kg \cdot K}$
Chemical	$LiFePO_4$
Normal capacity	58Ah
Normal voltage	3.7V
Operating temperature	−30 to 60 °C
Internal resistance	0.008Ω
Volume of cell	0.368L
Mass of Cell	830g

**Table 2**

The thermophysical properties of RT44 with 5 % SWCNT concentration [29,35].

$\rho \left( \frac{\text{kg}}{\text{m}^3} \right)$	$k \left( \frac{\text{W}}{\text{mK}} \right)$	$C_p \left( \frac{\text{J}}{\text{kgK}} \right)$	$\beta \left( \frac{1}{\text{K}} \right)$	$\mu \left( \frac{\text{kg}}{\text{ms}} \right)$	$T_m \text{ (K)}$	$T_{mr} \text{ (K)}$	$h \left( \frac{\text{W}}{\text{kg}} \right)$
842.5	0.731	1757	$2.2 \times 10^{-3}$	$9.1 \times 10^{-3}$	316	3	237.5

influential parameters affecting cooling performance are PCM material (35.4 %), PCM thickness (35.13 %), heat transfer coefficient (13.98 %), and additive percentage (5.09 %). The combination of Capric acid and RT-35 achieves the minimum cell temperature (303.088 K). A study [18] investigated the optimization of PCM in passive BTMS to achieve efficient and compact designs. The study identifies that paraffin wax with a transition temperature of 48 °C is most suitable. The use of a battery interval of 4.4 mm, a convective heat transfer coefficient of 0.8 W/m2/K, and a mass fraction of 10.9 % for expanded graphite in the PCM not only meets thermal safety requirements but also achieves a notable reduction in the volume fraction of the PCM by 18.4 %. Despite these advantages, the application of PCMs in BTMS has faced challenges related to their slow response times and limited thermal conductivity. To address these limitations, NePCMs have emerged as a promising solution. NePCMs incorporate nanoparticles into the PCM matrix, enhancing their thermal conductivity and reducing response times [19–21].

Nanoparticles, with their unique physicochemical properties and high surface-to-volume ratio, can significantly alter the behavior of fluids and offer numerous benefits across various applications. One crucial area where the addition of nanoparticles to fluids has proven beneficial is in BTMS [22–24]. Heat transfer plays a pivotal role in many industrial processes and electronic devices, and improving heat dissipation and thermal conductivity is of paramount importance. Nanoparticles, such as metal oxides, carbon nanotubes, graphene, and nano-encapsulated PCM, possess excellent thermal conductivity and specific heat capacity properties [25–27]. In this respect, by leveraging the unique properties of nanoparticles, NePCMs offer improved heat transfer capabilities and faster response times, making them well-suited for applications in hot climate conditions. In hot climates, such as the Arabian Peninsula, the need for efficient BTMS is particularly acute. The high ambient temperatures can significantly impact battery performance and safety,

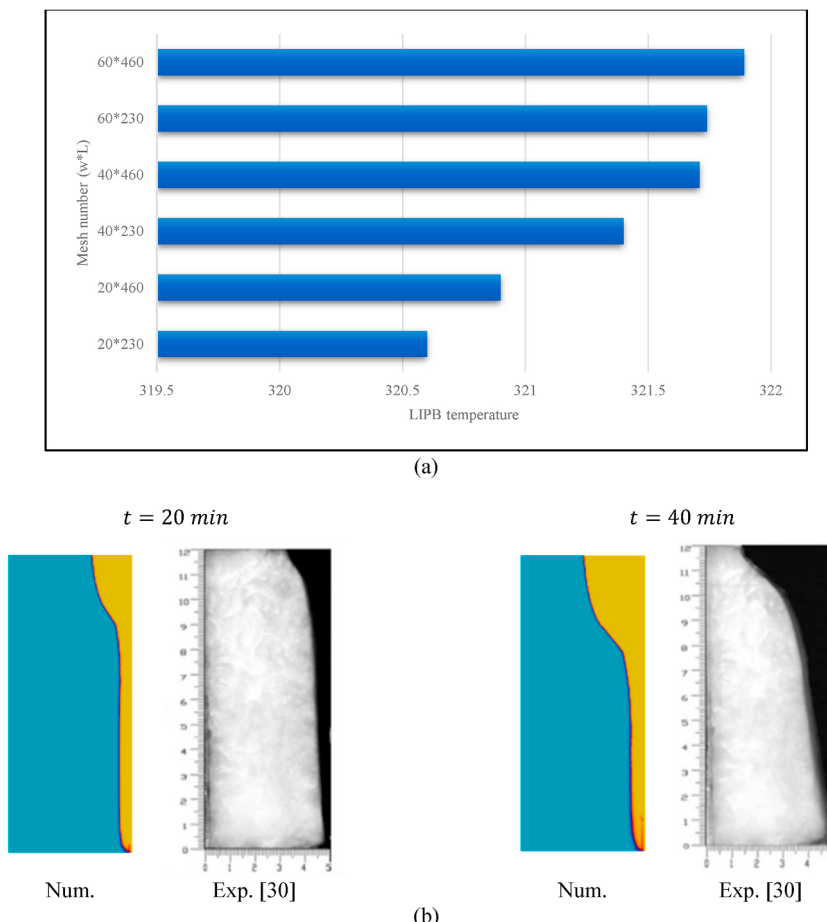
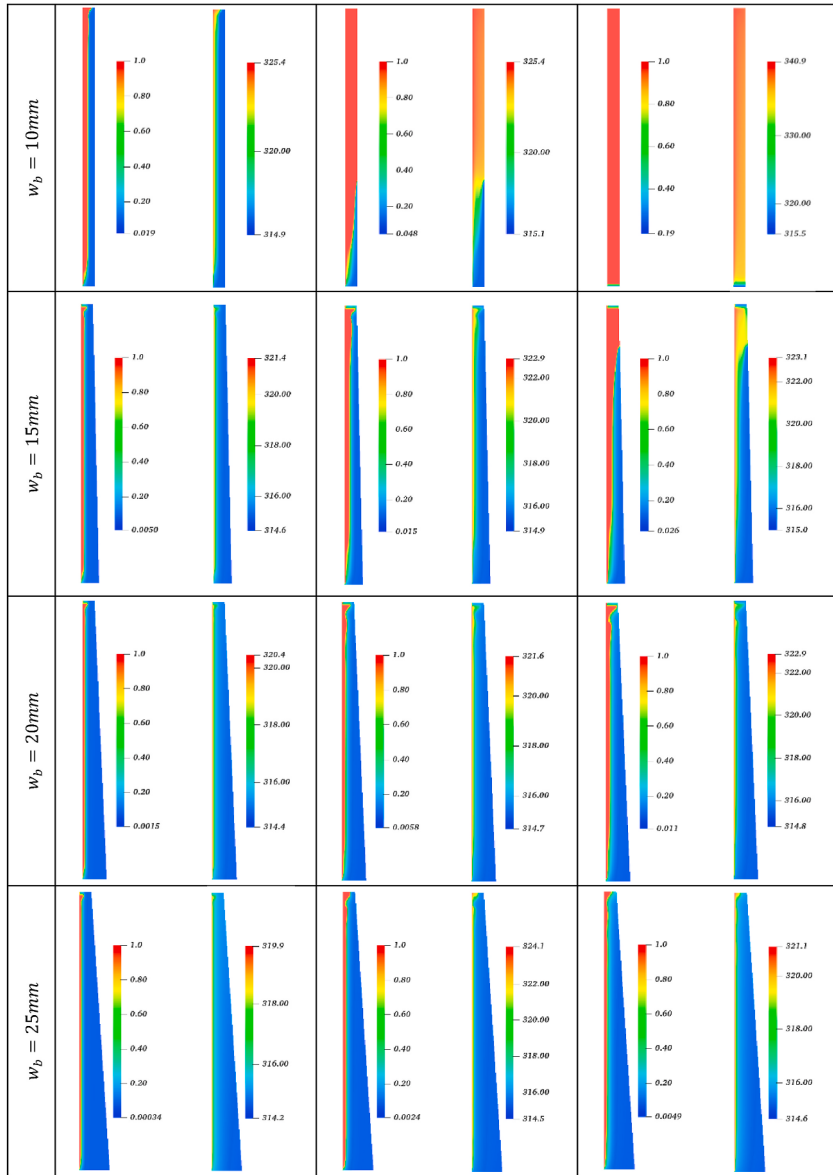


Fig. 2. a) The mesh independence analysis for the variations in LIPB temperature with respect to diverse mesh sizes at SOC = 100 % and b) a comparison of the melting fraction between the outcomes of our study and the research conducted by Kamkari et al. [36].



**Fig. 3.** The melting process and temperature distribution of NePCM for various  $w_b$  and  $w_t = 10$  mm at different SOCs.

making effective thermal control essential for maintaining battery health and longevity. The use of NePCMs in hot climates offers several advantages [28–31]:

- **Reduced Overheating Risk:** NePCMs effectively absorb and dissipate heat, minimizing the risk of battery overheating, even in harsh environmental conditions.
- **Improved Battery Performance:** Stable temperature control enables batteries to operate at their peak performance, extending their lifespan and reducing the risk of premature failure.
- **Enhanced Safety:** NePCMs contribute to safer battery operation by mitigating the risk of thermal runaway, a potentially catastrophic event that can lead to fires or explosions.

A study [32] presented a hybrid active and passive for BTMS using a combination of Thermoelectric Elements (TEE) and PCM in hot environments. In hot environments, PCM undergoes a phase transition to store the heat generated during battery discharge as latent heat, while TEE provides refrigeration effects to prevent PCM saturation. Results demonstrated that the combined effect of Composite PCM and TEE can keep the maximum battery temperature below 318.15 K during high-rate (3C) discharge in hot environments. Notably, the combination of TEE and CPCM reduces the maximum battery temperature by approximately 10 K compared to PCM cooling alone, showcasing improved cooling performance. Weng et al. [33] focused on advanced BTMS for electric vehicles, combining liquid cooling (LC) with PCM cooling for secondary heat dissipation. The thermal behaviors of tubular PCMs were investi-

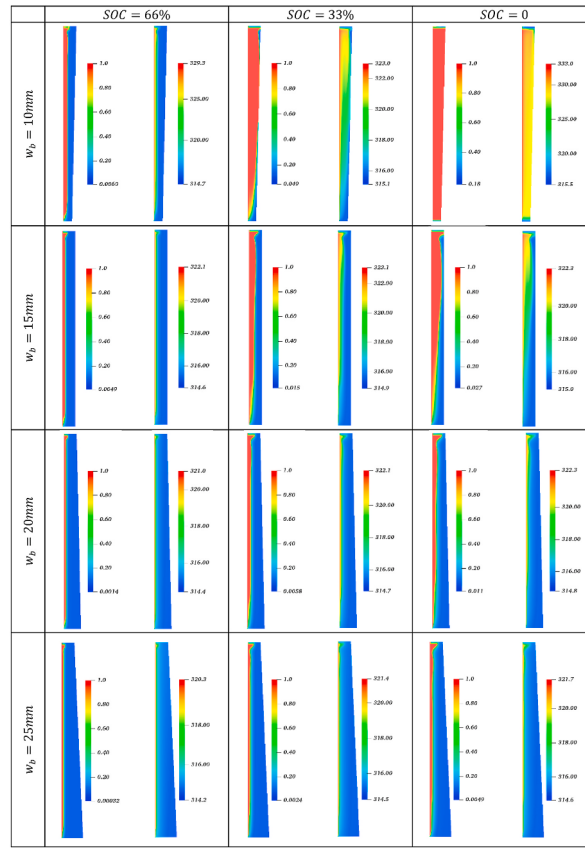


Fig. 4. The melting process and temperature distribution of NePCM for various  $w_b$  and  $w_t = 15$  mm at different SOCs.

gated under different liquid temperatures (25, 45, and 65 °C) to simulate various operating conditions of battery modules. Experimental results demonstrated the superior cooling effect of the PCM-CP module, even at high temperatures. A study [34] focused on temperature control in lithium-ion batteries using a composite of PCM and aluminum wire mesh plates in extreme environments. The aim is to mitigate temperature rise in high-temperature regions (50–55 °C) to prevent performance degradation and potential hazards. Polyethylene Glycol 1000 (PEG1000) with a melting point of 35–40 °C is used as the PCM, while aluminum wire mesh plates enhance thermal conductivity and temperature uniformity. Results demonstrated that incorporating PCM and aluminum wire mesh plates reduces surface temperatures significantly, improving battery pack performance. At ambient temperature, the maximum cell surface temperatures are reduced by 19 %, 21 %, and 26 % for discharge rates of 1 C, 2 C, and 3 C, respectively.

This research paper aimed to investigate the potential of NePCMs, specifically RT44 and SWCNT, for battery BTMS in hot climates. As the adoption of electric vehicles (EVs) and renewable energy systems gains significant traction in this region, the importance of efficient BTMS becomes paramount. The study aimed to explore the effects of varying the thicknesses of the top and bottom NePCM chamber on different parameters related to heat dissipation and temperature regulation. By examining the impact of different NePCM thicknesses, the researchers seek to optimize the design and configuration of the BTMS. This optimization is crucial for achieving efficient heat dissipation, mitigating overheating risks, and ensuring safe and reliable battery operation. The findings of this study will provide valuable insights into the potential of NePCMs to revolutionize BTMS in hot climates. The implications of this research extend beyond Saudi Arabia, as other regions with similar climatic conditions can benefit from the outcomes. The widespread adoption of EVs and renewable energy infrastructure relies heavily on addressing the challenges associated with BTMS in hot climates. By understanding the effectiveness of NePCMs and their optimal design configurations, this study contributes to advancing the adoption of sustainable transportation and clean energy solutions not only in Saudi Arabia but also in other comparable regions.

## 2. Schematic and properties

This study aimed to investigate the BTMS of lithium-ion pouch batteries (LIPBs) by utilizing multiple NePCM chambers arranged together to form a battery pack suitable for various applications (refer to Fig. 1). To conduct a comprehensive numerical analysis, one specific NePCM chamber was selected for simulation, as depicted on the right side of Fig. 1. The NePCM used in this study consisted of RT44 as the base material, with a 5 % concentration of Single-Walled Carbon Nanotubes (SWCNT) incorporated to enhance its cooling properties. The C-rate, representing the charge and discharge rate, was maintained at a constant value of 2C, equivalent to 116A. The ambient temperature was set to reflect the real conditions of Saudi Arabia, with a value of 40°C. This ambient temperature was

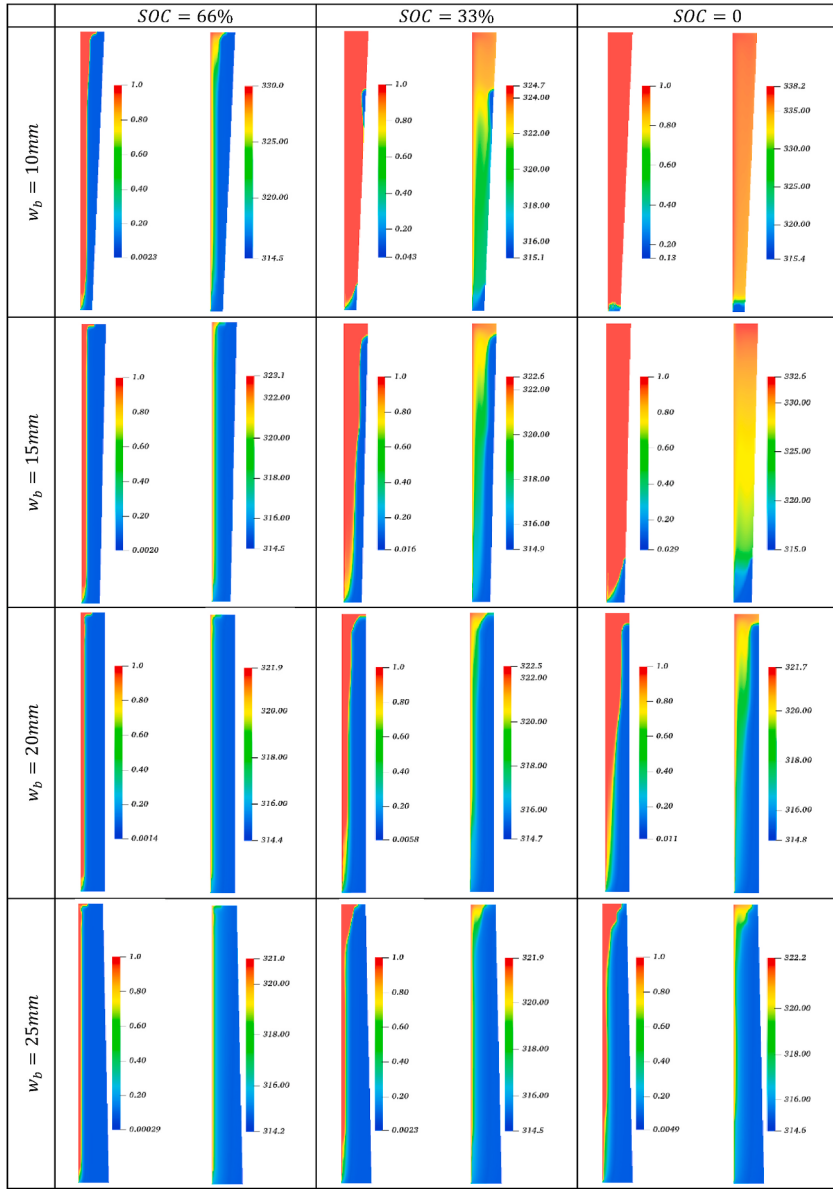


**Fig. 5.** The melting process and temperature distribution of NePCM for various  $w_b$  and  $w_t = 20$  mm at different SOCs.

also adopted as the initial temperature for the LIPB within the NePCM chamber. Furthermore, the study accounted for convective heat transfer ( $h_a = 2.5 \text{ W/m}^2\text{K}$ ) resulting from the ambient air surrounding the NePCM chamber. The walls of the chamber were assumed to be in contact with the ambient air, which shared the same temperature as the ambient environment ( $T_a = 40^\circ\text{C}$ ). Finally, Table 1 presents the key specifications of the LIPBs used in this study, specifically chosen to be suitable for operation in hot environments.

### 3. Methodology

To simulate the current study, several assumptions were made to simplify the modeling process. These assumptions include:

- **Incompressible and Laminar Flow:** It was assumed that the NPCM flows in an incompressible manner and exhibits laminar flow behavior. This assumption allows for the use of simplified fluid flow equations.
- **Constant Thermal Properties:** The thermal properties of the NPCM were considered constant throughout the simulation. This assumption implies that the specific heat capacity, thermal conductivity, and other thermal properties do not vary with temperature or phase change.

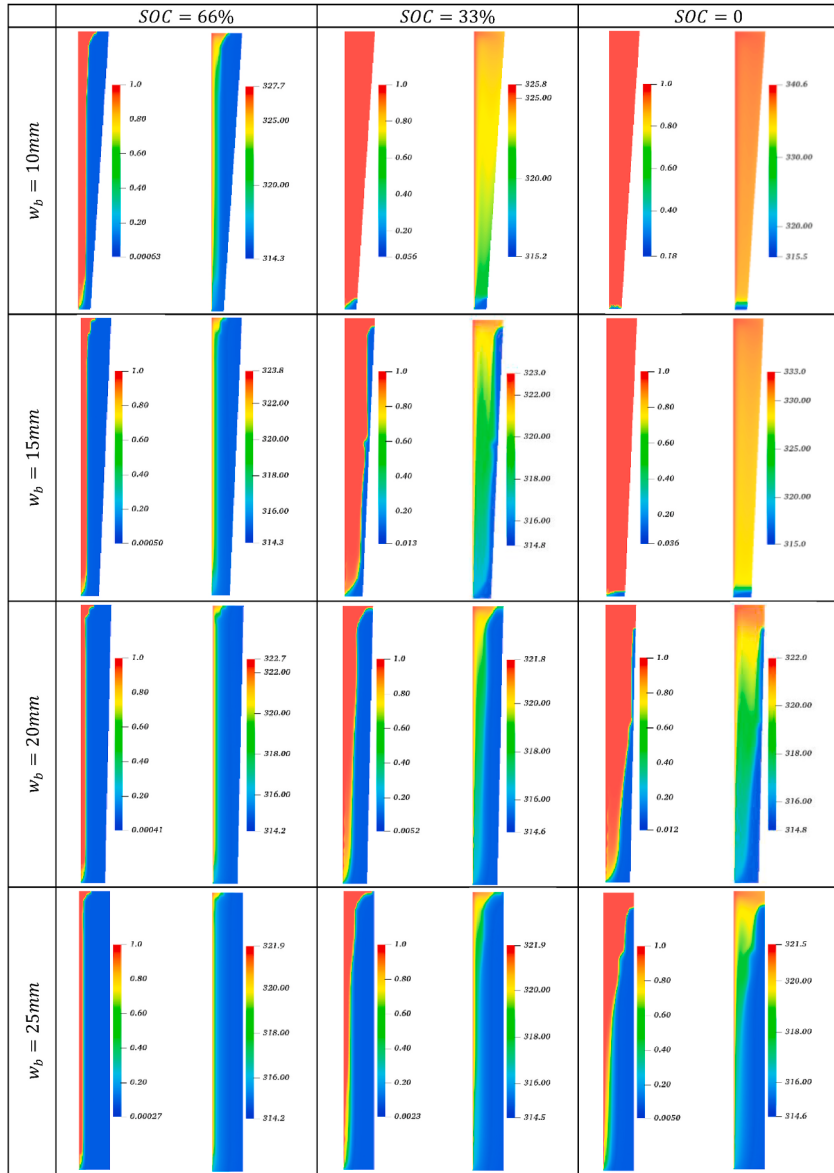


Fig. 6. The melting process and temperature distribution of NePCM for various  $w_b$  and  $w_t = 25$  mm at different SOCs.

- **Liquid-Solid Transition and Buoyant Force:** Two additional terms were incorporated into the momentum equations to account for the liquid-solid transition during phase change and the buoyant force resulting from density variations. These terms enable the modeling of the phase change process and the effects of density differences within the system.

Also, to capture the impact of turbulent eddies on heat and mass transfer, the Reynolds-Averaged Navier-Stokes (RAS) model was employed to determine turbulent dynamic viscosity and thermal conductivity. These parameters were essential for the momentum and energy equations. The  $k - \epsilon$  model from RAS was utilized to compute these parameters. Based on these assumptions, equations can be formulated as follows:

Mass equation:

$$\nabla \cdot \mathbf{V} = 0 \quad (1)$$

Momentum Equation:

$$\rho_{NePCM} \frac{\partial \mathbf{V}}{\partial t} + \rho_{NePCM} (\mathbf{V} \cdot \nabla) \mathbf{V} = -\nabla p + \mu_{NePCM} \nabla \cdot (\nabla \mathbf{V}) + (\rho \beta)_{NePCM} (T - T_s) \mathbf{g} - 10^5 \frac{(1 - \lambda)^2}{\lambda^3 + 10^{-3}} \mathbf{V} \quad (2)$$

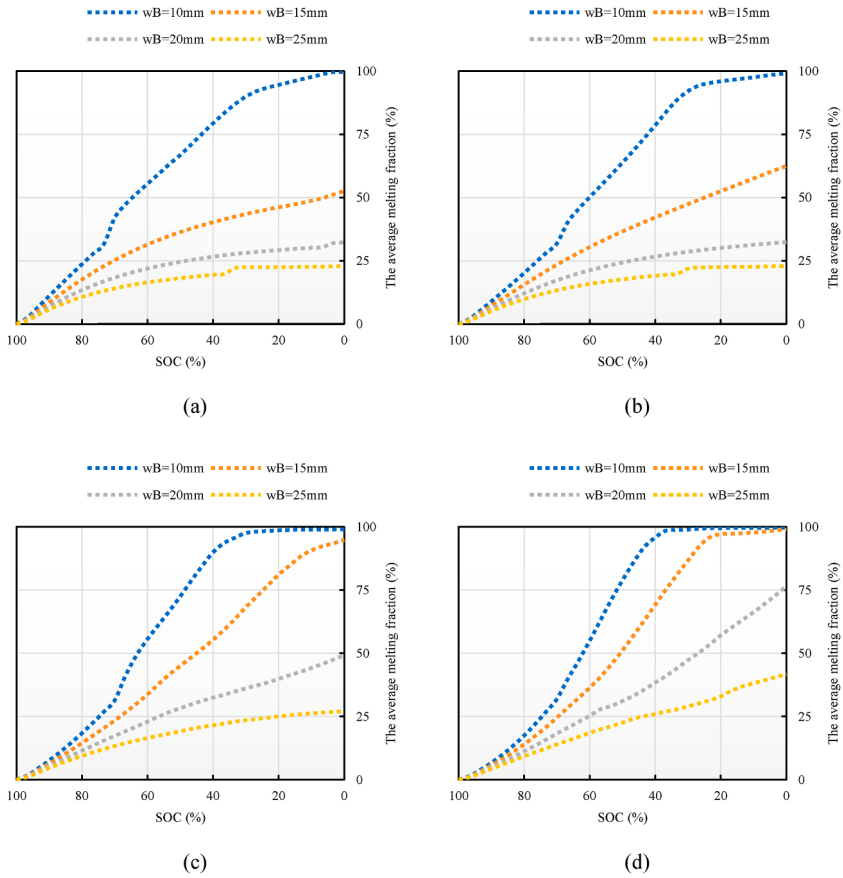


**Fig. 7.** The average melting fraction of NePCM versus SOC for a)  $w_t = 10\text{ mm}$ , b)  $w_t = 15\text{ mm}$ , c)  $w_t = 20\text{ mm}$ , and d)  $w_t = 25\text{ mm}$ .

Kinetic energy equation:

$$\frac{D}{Dt} (\rho_{NePCM} K) = \nabla \cdot (\rho_{NePCM} D_k \nabla K) + P - \rho_{NePCM} \varepsilon \quad (3)$$

Energy dissipation rate equation:

$$\frac{D}{Dt} (\rho_{NePCM} \varepsilon) = \nabla \cdot (\rho_{NePCM} D_\varepsilon \nabla \varepsilon) + \frac{C_1 \varepsilon}{K} \left( P + \frac{2}{3} K C_3 \nabla \cdot V \right) - \rho_{NePCM} C_2 \frac{\varepsilon^2}{K} \quad (4)$$

$$\mu_t = \rho_{NePCM} C_\mu \frac{K^2}{\varepsilon}, k_t = \frac{\mu_t C_{p,NePCM}}{Pr_t}$$

Where  $\rho$  is the density of the NPCM;  $V$  is the velocity vector;  $t$  is time;  $P$  is the pressure;  $\mu$  is the dynamic viscosity;  $g$  is the gravitational acceleration;  $T$  is temperature;  $\lambda$  is melting fraction;  $K$  is kinetic energy;  $\varepsilon$  is energy dissipation rate. turbulent parameters are  $C_1 = 1.44$ ,  $C_2 = 1.92$ ,  $C_3 = 0$ ,  $C_\mu = 0.09$ , and  $Pr_t = 0.85$ . Additionally, due to the inclusion of the liquid-solid transition, the effects of latent heat must be considered in the energy equation. The energy equation can be formulated as follows:

Energy equation:

$$\rho_{NePCM} \left( C_{p,NePCM} + h_{NPCM} \frac{d\lambda}{dT} \right) \frac{\partial T}{\partial t} + (\rho C_p)_{NePCM} (V \cdot \nabla T) = k_{NePCM} \nabla \cdot (\nabla T) \quad (5)$$

$$\lambda = 0.5 \operatorname{erf} \left( 4 \frac{T_s - T_m}{T_l - T_s} \right) + 0.5 \quad (6)$$

Where  $C_p$  is the specific heat capacity at constant pressure;  $k$  is the thermal conductivity;  $T_s$  is the temperature of the solid phase;  $T_l$  is the temperature of the liquid phase;  $T_m$  is the melting point. In this CFD simulation, the lumped thermal capacity model (LTCM) was utilized for determining the temperature of the LiFePO<sub>4</sub> Li-ion pouch cell (LIPC). The LTCM operates under the assumption that the battery's temperature is evenly spread across its entire volume, a premise supported by a low Biot number, signifying efficient and rapid heat transfer. Also, Table 2 shows the thermophysical properties of RT44 with 5 % SWCNT concentration.

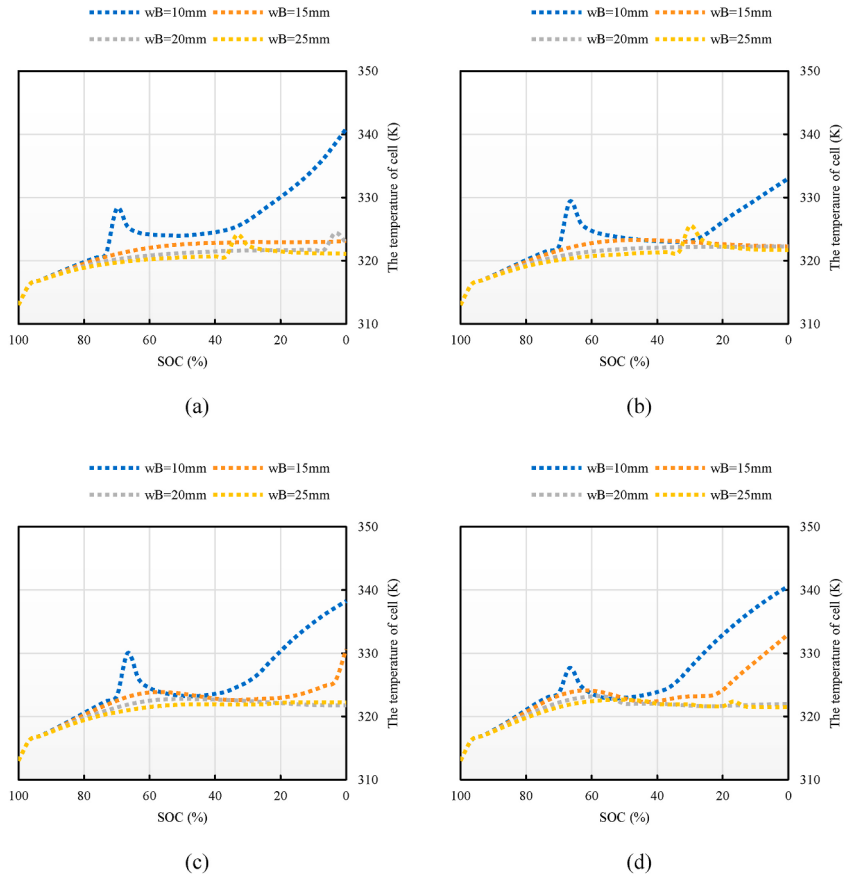


**Fig. 8.** The LIPB temperature versus SOC for a)  $w_t = 10\text{ mm}$ , b)  $w_t = 15\text{ mm}$ , c)  $w_t = 20\text{ mm}$ , and d)  $w_t = 25\text{ mm}$ .

#### 4. CFD settings

This research paper presents a comprehensive investigation of the effectiveness of NePCMs for BTMS in hot climates, focusing on the application of NePCMs made from RT44 and SWCNT in Saudi Arabia. A numerical study was conducted using computational fluid dynamics (CFD) to model the thermal behavior of a battery pack with NePCM chambers. The simulation employed the finite volume method (FVM) to accurately capture the dynamics of solid-liquid phase transitions and buoyancy effects, considering the effects of various thicknesses of the top and bottom of the NePCM chamber on the thermal performance. The PISO algorithm was utilized for pressure-velocity coupling, and the energy equation was solved to determine the temperature distribution. First-order upwind and second-order central schemes were employed for the discretization of the convective and conductive terms, respectively, ensuring accurate and efficient numerical solutions. The Courant number was controlled lower than the unit to maintain numerical stability throughout the simulation.

Upon establishing the numerical methods and schemes, the next phase in the CFD process involves meshing the geometry. In this study, structured meshes were utilized to represent the geometry that its top and bottom can be different in some samples. To guarantee the reliability of the results, mesh independence analysis was carried out under specific conditions of complete LIPB discharge, and  $w_b = w_t = 20\text{ mm}$ . The outcomes of this analysis are presented in Fig. 2 (a), illustrating the variations in LIPB temperature with respect to diverse mesh sizes. This analysis served to determine the level of mesh refinement necessary for precise and reliable results, ensuring that the chosen mesh resolution adequately captures the flow and temperature gradients within the NePCM and LIPB. The melting process of lauric acid as a PCM in a rectangular chamber was experimentally studied by Kamkari et al. [36]. In their experiment, one wall of the chamber was maintained at a constant temperature of 70 °C, while the other walls were insulated. The researchers captured images of the melting process and compared them with the results obtained from the present numerical simulation. Fig. 2 (b) presents the findings of both the simulation and experimental study [36], aiming to validate the accuracy of the numerical solution employed in this research. The results depicted in Fig. 2 (b) demonstrate a close agreement between the current numerical simulation and the experimental outcomes. This consistency between the two sets of results supports the reliability and effectiveness of the numerical approach used in this study.

## 5. Results and analysis

In this study, the effects of varying thicknesses (10 mm, 15 mm, 20 mm, and 25 mm) of the top and bottom NePCM chamber were investigated, specifically under a 2C charging rate. The objective was to explore the importance of these thickness values on several crucial parameters related to battery thermal management. Each parameter plays a significant role in understanding the behavior and performance of the NePCM system. Firstly, the distribution of the phase change process is a key parameter to consider. The thickness of the NePCM chamber can influence how the phase change occurs within the system. By examining the effects of different thicknesses, researchers can determine the distribution of heat transfer and phase change throughout the NePCM chamber, which is crucial for efficient and uniform cooling of the battery. Secondly, the NePCM temperature is a critical factor to monitor. The thickness of the NePCM chamber can affect the overall temperature of the NePCM material during charging. Understanding how different thicknesses impact NePCM temperature helps in optimizing the design and configuration of the thermal management system to ensure that the NePCM operates within the desired temperature range, enhancing its effectiveness in mitigating battery overheating. The average melting fraction is another parameter of interest in this study. It provides insights into the extent of phase change occurring within the NePCM chamber. By investigating the impact of different thicknesses on the average melting fraction, researchers can determine the amount of energy absorbed or released during the charging process, which is essential for evaluating the thermal performance and energy storage capacity of the NePCM system. Additionally, the temperature of the LIPB plays a crucial role in battery performance and safety. The thickness of the NePCM chamber can influence the temperature of the LIPB electrode, which can have implications for battery efficiency, cycling stability, and overall lifespan. Analyzing the effects of different thicknesses on the LIPB temperature provides valuable insights into the effectiveness of NePCM in regulating and maintaining optimal operating conditions for the battery. Lastly, investigating the impact of different thicknesses at various state-of-charges (SOCs) is vital. SOC refers to the amount of energy stored in the battery relative to its maximum capacity. By examining the behavior of the NePCM system at different SOC levels, researchers can understand how the thickness of the NePCM chamber affects the thermal management performance at various stages of battery operation. This knowledge is crucial for developing effective strategies that account for the dynamic behavior of the battery during different charge and discharge cycles. Overall, by analyzing the effects of different thicknesses of the NePCM chamber on the distribution of the phase change process, NePCM temperature, average melting fraction, and LIPB temperature at various SOCs, this study provides valuable insights into the importance of each parameter for optimizing battery thermal management. These findings contribute to the development of more efficient and reliable thermal management strategies, ensuring the safe and efficient operation of batteries in diverse applications.

**Fig. 3** depicts melting fraction and temperature contours at  $w_t = 10 \text{ mm}$  for different SOCs and wall thicknesses ( $w_b$ ) on one side of the NePCM chamber, specifically the right side. The melting fraction contours reveal that a layer of liquid NePCM formed near the battery's wall, rising against gravitational acceleration due to buoyant force. The NePCM started melting from the top of the chamber and moved downward, particularly noticeable at  $w_b$  values of 10 mm and 15 mm in low SOCs. When  $w_b$  was 10 mm and SOC was 0, the NePCM completely melted due to strong heat dissipation. In contrast, with  $w_b$  set at 15 mm, only a portion of the solid PCM melted as heat dissipation was consumed in warming the PCM. Conversely, the solid PCM did not melt in cases where  $w_b$  was 20 mm and 25 mm, likely due to the significant volume of the PCM. Temperature contours followed similar patterns to melting fraction contours, except at the solid-liquid boundary. Increasing  $w_b$  led to a reduction in PCM temperature since heat dissipation from the battery was utilized to warm the PCM rather than melting it. The most significant effect of increasing  $w_b$  from 10 mm to 15 mm was observed, resulting in a temperature decrease from 340.9 K to 323.1 K at a SOC of 0.

**Fig. 4** illustrates the melting process and temperature distribution of the NePCM for a wall thickness of the chamber's top ( $w_t$ ) of 10 mm. While the contour patterns in **Fig. 4** are similar to those in **Fig. 3**, there are some slight differences between them. In the first column, an increase in  $w_t$  resulted in a reduction of the liquid PCM layer adjacent to the LIPB wall, as the volume of the NePCM was raised and caused more heat dissipation to warm the NePCM chamber. Additionally, the maximum temperature at  $w_t = 10 \text{ mm}$  in **Fig. 4**, at a SOC of 0, was 7.9 K cooler compared to that in **Fig. 3** because this temperature difference can be attributed to the larger volume of NePCM in **Fig. 4**. However, no significant differences were observed for other  $w_t$  values. In summary, the maximum temperature at the end of discharge showed only slight variations of 0.8 K, 0.6 K, and 0.6 K between **Figs. 3 and 4** for  $w_t$  values of 15 mm, 20 mm, and 25 mm, respectively.

**Figs. 5 and 6** present the NePCM melting process and temperature distribution for wall thicknesses ( $w_t$ ) of 20 mm and 25 mm in the chamber's top, respectively. Upon comparing these figures with **Figs. 3 and 4** at  $w_b = 10 \text{ mm}$ , increasing  $w_t$  from 15 mm to 20 mm and 25 mm resulted in a change in the maximum temperature at SOC = 0 by -2.7 K and -0.3 K, respectively. Contrary to  $w_t = 15 \text{ mm}$ , increasing  $w_t$  to 20 mm and 25 mm at  $w_b = 10 \text{ mm}$  did not have a significant effect on temperature, as the increase in thermal resistance from conductivity outweighed the increment in PCM thickness at the top. Furthermore, increasing  $w_t$  from 10 mm to 20 mm and 25 mm elevated the maximum temperature by 9.5 K and 11.7 K, respectively. Notably, changes in  $w_t$  did not have a remarkable impact on the maximum temperature.

**Fig. 7** illustrates the average melting fraction of the NePCM for different thicknesses at the top and bottom of the chamber. The figure demonstrates that decreasing SOC enhanced the melting fraction as the released heat from the battery was utilized for sensible and latent heat. At  $w_b = 10 \text{ mm}$ , the NePCM was completely melted for all  $w_t$  values when the battery was fully discharged. However, it was observed that the NePCM melted earlier for  $w_t = 20 \text{ and } 25 \text{ mm}$  compared to  $w_t = 10 \text{ and } 15 \text{ mm}$ . In **Fig. 7a**, for  $w_t = 10 \text{ mm}$ , an increase in  $w_b$  from 10 mm to 15 mm, 20 mm, and 25 mm resulted in a reduction of the average melting fraction from 100 % to 52 %, 32 %, and 22.8 %, respectively. This reduction was due to the increase in NePCM volume resulting from the increased  $w_b$ , while heat dissipation remained relatively constant. Similar trends were observed for other  $w_t$  values, albeit with lower reductions, as the released heat was consumed for melting instead of warming and releasing to the ambient environment due to the increased thermal re-

sistance associated with thicker PCM layers. For example, increasing  $w_t$  from 10 mm to 25 mm at  $w_b = 25 \text{ mm}$  increased the melting fraction from 22.8 % to 41.7 %. It is important to note that the effects of ambient convective heat transfer ( $h_a = 2.5 \text{ W/m}^2\text{K}$  and  $T_a = 40^\circ\text{C}$ ) should not be disregarded, as their influence is directly related to the chamber thickness. Therefore, their impact is more significant when the thickness of the chamber is lower, such as 10 mm.

Fig. 8 provides insights into the impact of different parameters on the temperature of the LIPB temperature during the discharge process. For all  $w_t$  values and  $w_b = 10 \text{ mm}$ , a peak in LIPB temperature was observed at SOC = 70 %. This can be attributed to the thickness of the liquid NePCM near the LIPB wall and the influence of convective heat transfer from the ambient environment. Furthermore, the LIPB temperature exhibited a significant increase after reaching SOC = 60 %, as a substantial amount of NePCM had melted and the remaining heat dissipation was utilized for sensible heat or to raise the temperature of the NePCM, directly affecting the LIPB temperature. When  $w_t$  was 10 mm and 15 mm at  $w_b = 15 \text{ mm}$ , the LIPB temperature gradually increased up to 322 K at SOC = 0. However, for  $w_t = 20 \text{ and } 25 \text{ mm}$ , the LIPB temperature experienced a sudden increase up to 330 K at SOC = 16 % and 23 %, respectively. This abrupt rise can be attributed to the complete melting of the liquid NePCM and the influence of the ambient environment. Additionally, for all  $w_t$  values at  $w_b = 20 \text{ and } 25 \text{ mm}$ , the LIPB temperature exhibited a smooth increase ranging from 320 K to 325 K.

## 6. Conclusion

In this study, the application of NePCM for BTMS in the hot climate of Saudi Arabia was investigated. The effects of different thicknesses of the NePCM chamber's top and bottom on the phase change process, NePCM temperature, average melting fraction, and LIPB temperature were examined at various SOCs. The results showed that the thickness of the NePCM chamber wall played a crucial role in the melting process and temperature distribution. Increasing the thickness of the chamber's bottom adjacent to the LIPB ( $w_b$ ) resulted in a reduction of the average melting fraction, as more heat was used for warming rather than melting the NePCM. Similarly, increasing the thickness of the chamber's top ( $w_t$ ) led to a decrease in the liquid PCM layer adjacent to the LIPB wall, as more volume was occupied by the NePCM, affecting the heat dissipation and temperature distribution. The maximum temperature at SOC = 0 showed slight variations depending on the  $w_t$  and  $w_b$  values. Changes in  $w_t$  had a minimum impact on the maximum temperature, while increasing  $w_b$  from 10 mm led to a notable decrease in the maximum temperature. In contrast to imagining that an increment of NePCM thickness can regulate battery temperature, NePCM thickness had no meaningful impact on battery temperature because of the importance of the ambient environment. These findings emphasize the importance of optimizing the thicknesses of the NePCM chamber walls and considering the effects of the ambient environment for efficient BTMS in hot climates. By carefully designing the NePCM system, it is possible to regulate temperature distribution, enhance heat dissipation, and improve the safety and performance of LIPBs, ultimately contributing to their reliable operation in challenging environmental conditions.

## CRediT authorship contribution statement

**Jing Zhu:** Supervision, Conceptualization. **Rishabh Chaturvedi:** Formal analysis, Data curation. **Yasser Fouad:** Project administration, Funding acquisition. **Ibrahim Albaijan:** Resources, Methodology. **Nizomiddin Juraev:** Writing – original draft, Visualization, Validation. **Laith H. Alzubaidi:** Writing – review & editing, Writing – original draft, Investigation. **Ibrahim Mahariq:** Investigation, Writing – review & editing. **Abdulkareem Afandi:** Writing – review & editing, Resources. **Hakim AL. Garalleh:** Writing – original draft, Formal analysis.

## Declaration of competing interest

The authors declare that they have no known competing financial interests or personal relationships that could have appeared to influence the work reported in this paper.

## Data availability

The authors do not have permission to share data.

## Acknowledgement

The authors extend their appreciation to the Researchers Supporting Project number (RSPD2024R698), King Saud University, Riyadh, Saudi Arabia for funding this research work.

## References

- [1] A. Bar-Cohen, P. Wang, Thermal Management of On-Chip Hot Spot, 2012.
- [2] L.C. Jia, Z.X. Wang, L. Wang, J.F. Zeng, P.Y. Du, Y.F. Yue, L.H. Zhao, S.L. Jia, Self-standing boron nitride bulks enabled by liquid metals for thermal management, Mater. Horiz. 10 (12) (2023) 5656–5665.
- [3] B.B. Sui, L. Sha, P.F. Wang, Z. Gong, Y.H. Zhang, Y.H. Wu, L.N. Zhao, J.J. Tang, F.N. Shi, In situ zinc citrate on the surface of Zn anode improves the performance of aqueous zinc-ion batteries, J. Energy Storage 82 (2024) 110550.
- [4] J. Lin, X. Liu, S. Li, C. Zhang, S. Yang, A review on recent progress, challenges and perspective of battery thermal management system, Int. J. Heat Mass Tran. 167 (2021) 120834.
- [5] S. Yin, X. Ren, R. Zheng, Y. Li, J. Zhao, D. Xie, Y. Mei, Improving fire safety and mechanical properties of waterborne polyurethane by montmorillonite-passivated black phosphorus, Chem. Eng. J. 464 (2023) 142683.
- [6] Y. Du, X. Liu, L. Chen, S. Yin, Y. Xie, A. Li, X. Liang, Y. Luo, F. Wu, Y. Mei, D. Xie, 3D hierarchical fireproof gel polymer electrolyte towards high-performance and

- comprehensive safety lithium-ion batteries, *Chem. Eng. J.* 476 (2023) 146605.
- [7] W. Wu, S. Wang, W. Wu, K. Chen, S. Hong, Y. Lai, A critical review of battery thermal performance and liquid based battery thermal management, *Energy Convers. Manag.* 182 (2019) 262–281.
- [8] C. Zhu, Y. Hao, H. Wu, M. Chen, B. Quan, S. Liu, X. Hu, S. Liu, Q. Ji, X. Lu, J. Qu, Self-assembly of binderless MXene aerogel for multiple-scenario and responsive phase change composites with ultrahigh thermal energy storage density and exceptional electromagnetic interference shielding, *Nano-Micro Lett.* 16 (1) (2024) 57.
- [9] M. Gan, T. Lu, W. Yu, J. Feng, X. Chong, Capturing and visualizing the phase transition mediated thermal stress of thermal barrier coating materials via a cross-scale integrated computational approach, *J. Adv. Ceramics* (2024).
- [10] M.M. Heyhat, S. Mousavi, M. Siavashi, Battery thermal management with thermal energy storage composites of PCM, metal foam, fin and nanoparticle, *J. Energy Storage* 28 (2020) 101235.
- [11] T. Xin, S. Tang, F. Ji, L. Cui, B. He, X. Lin, X. Tian, H. Hou, Y. Zhao, M. Ferry, Phase transformations in an ultralight BCC Mg alloy during anisothermal ageing, *Acta Mater.* 239 (2022) 118248.
- [12] W. Kuang, H. Wang, X. Li, J. Zhang, Q. Zhou, Y. Zhao, Application of the thermodynamic extremal principle to diffusion-controlled phase transformations in Fe-CX alloys: modeling and applications, *Acta Mater.* 159 (2018) 16–30.
- [13] F. Chen, R. Huang, C. Wang, X. Yu, H. Liu, Q. Wu, K. Qian, R. Bhagat, Air and PCM cooling for battery thermal management considering battery cycle life, *Appl. Therm. Eng.* 173 (2020) 115154.
- [14] J. Wang, Z. Pan, Y. Wang, L. Wang, L. Su, D. Cuiuri, Y. Zhao, H. Li, Evolution of crystallographic orientation, precipitation, phase transformation and mechanical properties realized by enhancing deposition current for dual-wire arc additive manufactured Ni-rich NiTi alloy, *Addit. Manuf.* 34 (2020) 101240.
- [15] X. Long, K. Chong, Y. Su, L. Du, G. Zhang, Connecting the macroscopic and mesoscopic properties of sintered silver nanoparticles by crystal plasticity finite element method, *Eng. Fract. Mech.* 281 (2023) 109137.
- [16] F. Zhang, F. Lu, B. Liang, Y. Zhu, H. Gou, K. Xiao, Y. He, Thermal performance analysis of a new type of branch-fin enhanced battery thermal management PCM module, *Renew. Energy* 206 (2023) 1049–1063.
- [17] S. Sudhakaran, M. Terese, Y. Mohan, A.D. Thampi, S. Rani, Influence of various parameters on the cooling performance of battery thermal management systems based on phase change materials, *Appl. Therm. Eng.* 222 (2023) 119936.
- [18] S. Wang, D. Zhang, C. Li, J. Wang, J. Zhang, Y. Cheng, W. Mei, S. Cheng, P. Qin, Q. Duan, J. Sun, Numerical optimization for a phase change material based lithium-ion battery thermal management system, *Appl. Therm. Eng.* 222 (2023) 119839.
- [19] J. Alsarraf, A.A. Alnaqi, A.A. Al-Rashed, Effect of nanoparticles shape on the cooling process of a lithium ion battery in geometry with capillary channels in the presence of phase change material, *J. Energy Storage* 48 (2022) 103998.
- [20] X. Zheng, C. Han, C.S. Lee, W. Yao, C. Zhi, Y. Tang, Materials Challenges for aluminum ion based aqueous energy storage devices: progress and prospects, *Prog. Mater. Sci.* (2024) 101253.
- [21] X. Zhang, Y. Tang, F. Zhang, C.S. Lee, A novel aluminum-graphite dual-ion battery, *Adv. Energy Mater.* 6 (11) (2016) 1502588.
- [22] S. Mirshahi, B. Vahedi, K. Aryana, A. Sazgarnia, Cancerous cell viability affected by synergism between electric pulses and a low dose of silver nanoparticle: an adaptive neuro-fuzzy inference system, *Med. Novel Technol. Devices* 21 (2024) 100280.
- [23] M. Wang, C. Jiang, S. Zhang, X. Song, Y. Tang, H.M. Cheng, Reversible calcium alloying enables a practical room-temperature rechargeable calcium-ion battery with a high discharge voltage, *Nat. Chem.* 10 (6) (2018) 667–672.
- [24] R. Li, Y. Pan, X. Zhang, W. Dai, B. Liu, J. Li, Mechanical safety prediction of a battery-pack system under low speed frontal impact via machine learning, *Eng. Anal. Bound. Elem.* 160 (2024) 65–75.
- [25] B. Vahedi, E. Golab, A.N. Sadr, K. Vafai, Thermal, thermodynamic and exergoeconomic investigation of a parabolic trough collector utilizing nanofluids, *Appl. Therm. Eng.* 206 (2022) 118117.
- [26] E. Golab, S. Goudarzi, H. Kazemi-Varnamkhasti, H. Amigh, F. Ghaemi, D. Baleanu, A. Karimipour, Investigation of the effect of adding nano-encapsulated phase change material to water in natural convection inside a rectangular cavity, *J. Energy Storage* 40 (2021) 102699.
- [27] E. Golab, B. Vahedi, A. Jain, R.A. Taylor, K. Vafai, Laminar forced convection in a tube with a nano-encapsulated phase change materials: minimizing exergy losses and maximizing the heat transfer rate, *J. Energy Storage* 65 (2023) 107233.
- [28] A. Verma, S. Shashidhara, D. Rakshit, A comparative study on battery thermal management using phase change material (PCM), *Therm. Sci. Eng. Prog.* 11 (2019) 74–83.
- [29] M. Luo, J. Song, Z. Ling, Z. Zhang, X. Fang, Phase change material coat for battery thermal management with integrated rapid heating and cooling functions from – 40° C to 50° C, *Mater. Today Energy* 20 (2021) 100652.
- [30] A. Wazeer, A. Das, C. Abeykoon, A. Sinha, A. Karmakar, Phase change materials for battery thermal management of electric and hybrid vehicles: a review, *Energy Nexus* (2022) 100131.
- [31] Z.Y. Jiang, H.B. Li, Z.G. Qu, J.F. Zhang, Recent progress in lithium-ion battery thermal management for a wide range of temperature and abuse conditions, *Int. J. Hydrogen Energy* 47 (15) (2022) 9428–9459.
- [32] G. Liao, K. Jiang, F. Zhang, E. Jiaqiang, L. Liu, J. Chen, E. Leng, Thermal performance of battery thermal management system coupled with phase change material and thermoelectric elements, *J. Energy Storage* 43 (2021) 103217.
- [33] J. Weng, C. Xiao, X. Yang, D. Ouyang, M. Chen, G. Zhang, E.L. Waiming, R.K.K. Yuen, J. Wang, An energy-saving battery thermal management strategy coupling tubular phase-change-material with dynamic liquid cooling under different ambient temperatures, *Renew. Energy* 195 (2022) 918–930.
- [34] Y. Azizi, S.M. Sadrameli, Thermal management of a LiFePO<sub>4</sub> battery pack at high temperature environment using a composite of phase change materials and aluminum wire mesh plates, *Energy Convers. Manag.* 128 (2016) 294–302.
- [35] M. Fadl, P.C. Eames, An experimental investigation of the melting of RT44HC inside a horizontal rectangular test cell subject to uniform wall heat flux, *Int. J. Heat Mass Tran.* 140 (2019) 731–742.
- [36] B. Kamkar, H. Shokouhmand, F. Bruno, Experimental investigation of the effect of inclination angle on convection-driven melting of phase change material in a rectangular enclosure, *Int. J. Heat Mass Tran.* 72 (2014) 186–200.